STREAM

IST-1999-10341

STREAM CONSORTIUM:
CNR-LAMEL / ST Microelectronics / ISEN / SOFT IMAGING SYSTEM / University of Sheffield / IMEC / CNR-IESS / University of Perugia

DELIVERABLE D11

Workpackage WP3

Lead participant: CNR-IESS

A hardware/software set-up for XRD with the necessary characteristics of mechanical precision and stability

Main Author	S. Lagomarsino, CNR-IESS		
Contributing authors	A. Cedola, CNR-IESS		
Date:	28 02 2001	***Doc.No:***	IST10341-IE-RP001
Keywords:	X-ray micro-diffraction, Waveguide, Strain measurement, Synchrotron radiation		

Distribution list	**Project Officer:** B.Netange (3 copies) **All Partners:** A. Armigliato CNR-LAMEL G.P.Carnevale ST Microelectronics V. Senez ISEN T. Schilling Soft Imaging System A.G.Cullis USFD (University of Sheffield) I. De Wolf IMEC G. Carlotti UniPg (University of Perugia)

Table of contents

Abstract

In this Deliverable the x-ray micro-diffraction technique is described in detail. The optical element which is at the basis of this method, the x-ray waveguide, is preliminary presented. Then the whole experimental set-up is described and the alignment and measurement procedures are explained. The data analysis method is then critically presented together with examples of measurements on samples provided by ST. If many details are given is because this deliverable has also the purpose to serve as a kind of "instruction manual" for people who wants to perform micro-diffraction measurements with the WG and has no direct experience. What is described is the result of a development carried out on strict and fruitful collaboration with W. Jark and S. Di Fonzo of Sincrotrone Trieste.

1. The x-ray waveguide

The x-ray microdiffraction technique, object of this deliverable, is based on an innovative optical element for medium-high energy x-rays, i.e. the waveguide (WG) [1,2]. A typical x-ray WG structure (fig. 1) consists (from bottom to top) of an ultra-flat substrate, a metal layer few tens of nm thick (layer #3), a guiding layer made of a low-density material (for ex. C or Be) having a thickness of the order of 100 nm (layer #2) and a metal cap layer few nm thick (layer #1). When an x-ray beam impinges at grazing angle on this kind of structure, part of the intensity is totally reflected, but an evanescent wave penetrates the top (very thin) metal layer, it is refracted by the intermediate layer, and totally reflected at the interface between layers 2 and 3.

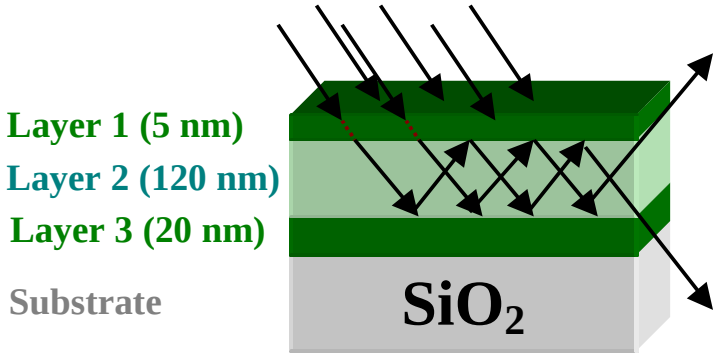

Figure 1. *Schematic view of a waveguide. Layer 2 (the guiding layer) must have a lower electron density than layers 1 and 3. In general layer 2 is C or Be, and layers 1 and 3 are metals (Cr, Ni or Mo).*

A strong x-ray standing wave (XSW) field inside the guiding layer is formed with the spatial periodicity depending on the incident angle. When the XSW periodicity is equal to an integer fraction of the layer thickness, a strong resonance takes place, with an enhancement of the electro-magnetic (e.m.) field hundredfold with respect to the incoming e.m. field intensity [3] (see fig. 2). In strict analogy with mode excitation in microwave resonators, the resonantly excited e.m. field can travel along the WG and exit at its end. Only when the resonance takes place an appreciable intensity can be measured at the exit of the WG. At the same time for these angles the reflected intensity is strongly depleted. Fig. 3 shows the reflected intensity and the guided one as a function of the external angle of incidence [4]. As can be seen several modes are excited, but for microdiffraction measurements we use in general only the first one.

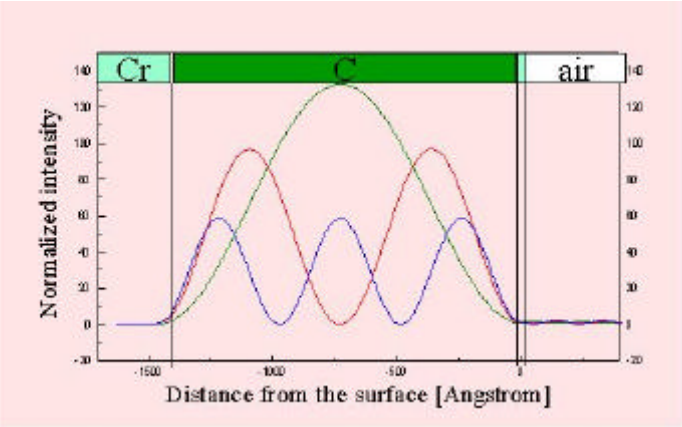

Figure 2. *Electromagnetic field intensity distribution inside a C guiding layer 140 nm thick cladded between two Cr layers in the first three resonance modes. Photon energy » 13 KeV.*

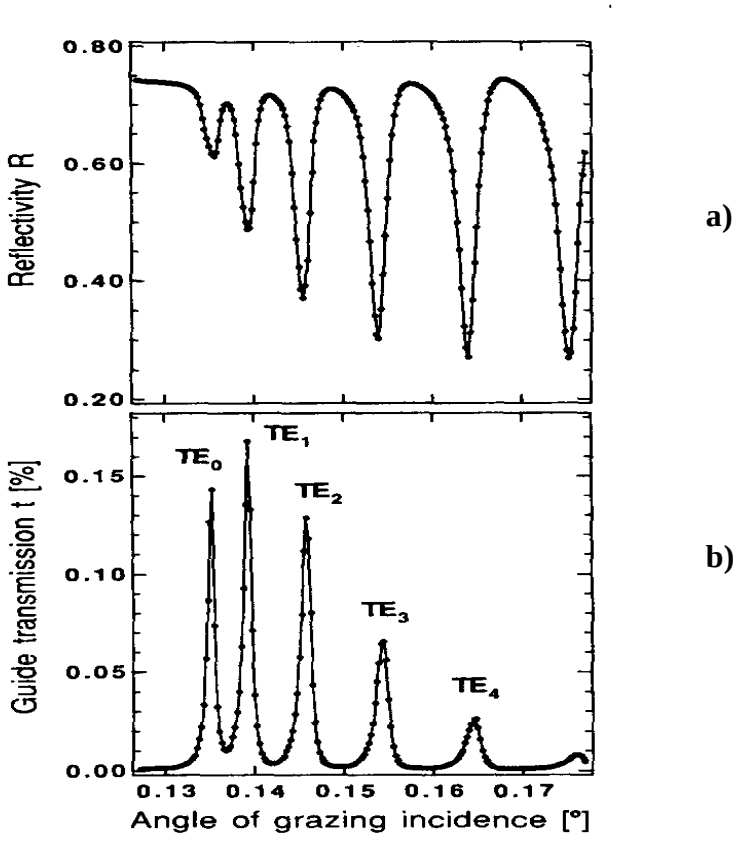

Figure 3. *Intensity of the reflected (a) and waveguided (b) beams as a function of the angle of incidence, normalised to the incoming beam intensity, for the same waveguide of fig. 2.*

1.1 Beam properties

The properties of the beam exiting the WG can be summarised as following (to simplify the discussion we consider a reference frame XYZ where X is the direction of the incoming x-ray beam, Y is horizontal and transverse to the beam, and Z the vertical co-ordinate. In this reference frame the WG surface lies in the XY plane):

i) the beam is confined in the Z direction, with a Full Width at Half Maximum (FWHM) equal to the half of the guiding layer thickness; typical values of FWHM are of the order of 40 - 70 nm;
ii) the exiting beam is divergent with a divergence of typically 1 mrad (≈wavelength/guiding layer thickness);
iii) the beam is highly coherent and can be approximated in the vertical direction by a gaussian beam, in strict analogy with a laser beam;
iv) in the XY plane the beam remains unaltered; if the incident beam is a plane wave then the beam exiting the WG is a cylindrical wave;
v) the gain (defined as the ratio between the flux density at the exit divided by the incoming flux density) has reached values of about one hundred in recent experiments, with an improvement of three orders of magnitude during the last three years [5]. Gain can be also understood as the increase in flux with respect to an hypothetical slit having an aperture equal to the FWHM guiding layer thickness value.

1.2 Physical WG characteristics

The efficiency (and therefore the gain) of the WG depends on several factors, and in particular on the materials used and on the degree of flatness, roughness and thickness homogeneity of the different layers. With the guiding layer in carbon, the resulting gain was of the order of 10 at the best. A strong improvement (one order of magnitude at least) has been obtained substituting Carbon with Berillium. This because the main loss inside the WG are due to photoelectric absorption into the guiding layer and to the reflection coefficient which is less than one (though very close). Substrate is a carefully polished 2" Si substrate (rms roughness of the order of 0.8 nm), with its end cut and shaped as an edge to facilitate the approaching of samples. The main parameters of the WG can be accurately determined by thorough analysis of the reflectivity curve. Fig. 4 shows the experimental reflectivity and the corresponding best fitting from which the individual layers thickness, the rms roughness of the interfaces and the incoming beam divergence can be determined [4].

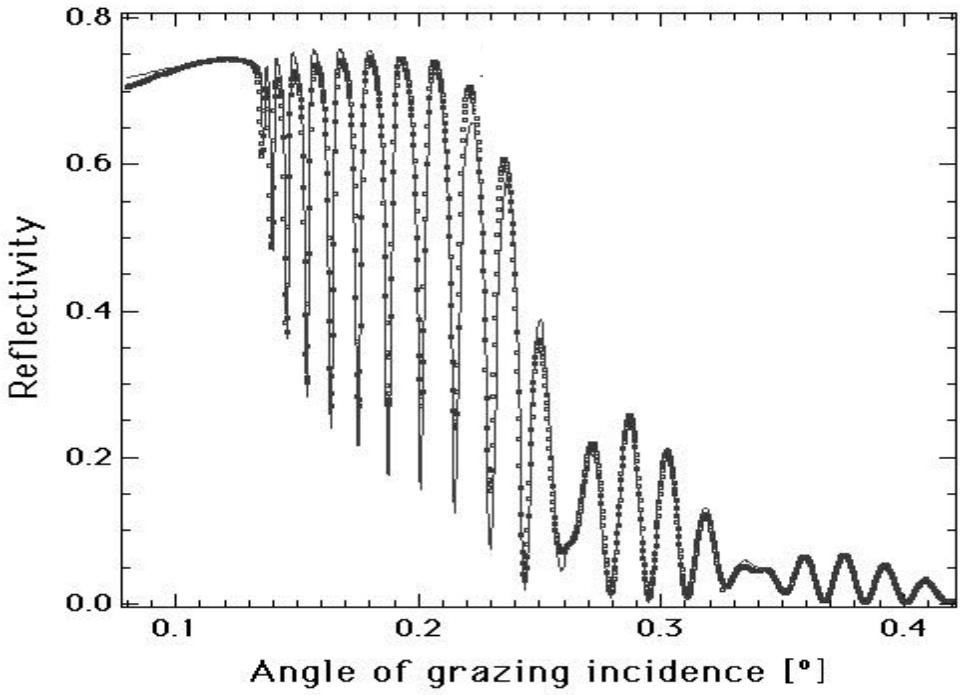

Figure 4. *Experimental reflectivity measurements (dots) and best-fitting (solid line) for a waveguide with (from bottom to top) a Cr layer 22 nm thick, a C layer 136.9 nm thick, and a top Cr layer 4.4 nm thick. rms surface roughness: 0.8 nm, incoming beam divergence* $s = 8.2$ *mrad*

2. Principle of micro-diffraction measurement

Two experimental arrangements can in principle be used to carry out microdiffraction measurements: a scanning geometry and a projection geometry. In both these procedures we exploit the characteristics of the WG that modifies the incident beam (size and divergence) only in the plane perpendicular to its surface. The beam properties in the plane parallel to its surface remain unaltered. Therefore, in the reference frame described before, if diffraction takes place with the scattering vector lying in the XY plane, the intrinsic properties of the synchrotron radiation (in particular its collimation) can be used. On the other side, we use the characteristics of the guided beam (its very small size and its divergence) to reach very good spatial resolution in the Z direction.

i) **Scanning geometry**; in this case the sample is brought as close as possible to the WG end, and is scanned vertically in order to illuminate only a small portion. At each vertical position a diffraction pattern is recorded. If the sample has a polycrystalline structure and the detector is a two-dimensional one, the diffraction pattern is recorded with just one exposure. If the sample is a monocrystal, then it is necessary to measure the diffracted intensity at different incident angles, thus recording what is called a "rocking curve". If the sample is very close to the WG exit, then the spatial resolution is equal to the beam size. Since the beam exiting the WG has a divergence of the order of 1 mrad, the spatial resolution

deteriorates as a function of the distance D_1 sample-WG, at a rate of about 1 μ per mm. At a reasonable distance D_1 of the order of 100 μ the deterioration is of the order of 100 nm.

ii) **Projection geometry**: in this case it is essential to use a position-sensitive detector, such as for example a CCD x-ray camera, and the coherence and divergence properties of the beam are exploited. The set-up is sketched in figure 5. Diffraction takes place in the horizontal plane, thus maintaining a very small divergence (few μrads). The CCD intercepts the diffracted beam at an angle 2θ and at a distance D_2 from the sample, giving a magnified view, in the vertical direction, of the diffracting region with a magnification $M \approx D_2/D_1$, where D_1 is the distance WG - Sample. In practice a one-to-one correspondence between the sample Z co-ordinate and the single CCD pixel can be done.

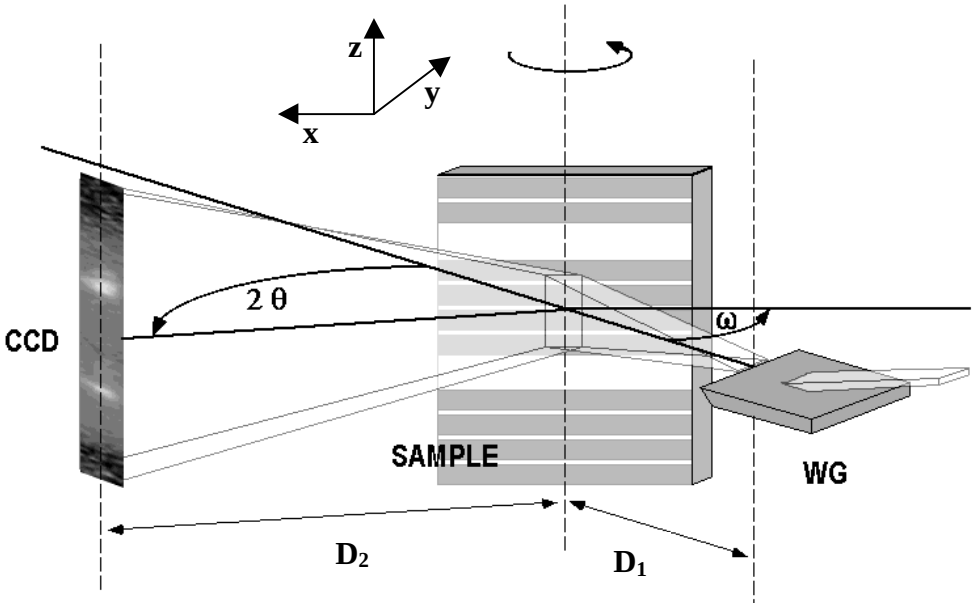

Figure 5. *Schematic set-up for microdiffraction experiments using a waveguide. The beam is compressed by the WG in the vertical direction, but remains unaltered in the horizontal one, thus allowing diffraction in the horizontal plane to be performed with a very good collimated beam.*

The advantage of the projection geometry is that the WG-sample distance is no more critical, because good magnification values (100÷1000) can be obtained with D_1 distances of the order of few mm. Moreover the spatial resolution, due to the coherence properties of the beam, can be in principle even better than the beam size. Geometrically the spatial resolution is given by the ratio between the pixel size and the magnification factor. In fact careful calculations of all the possible aberration effects should be carried out in order to establish precisely the spatial resolution obtainable. We have measured a resolution of 100 nm with a pixel size of about 10 μm and a magnification factor of 100 [6], but we estimate that this is not the ultimate limit. Another advantage is that the structural information are obtained simultaneously on the whole portion of the sample illuminated. This can be several microns (in Z), therefore in general an entire micro-structure can be examined without need of further scanning. The projection geometry can be adopted only with single crystals, therefore in order to measure their structural properties a diffraction profile (or Rocking Curve, RC) must be recorded. This is accomplished by rotating the crystal around a vertical axis (we recall here that the scattering plane lies in the XY plane), thus changing the incidence angle ω between the incoming beam and the diffracting plane. The CCD detector takes the image of the diffracted beam at each angular step, and the RC for each small

portion of the sample can be extracted with a proper analysis procedure. This will be described in detail later.

3. The experimental set-up

The experimental set-up is composed of several parts that must provide the possibility to:

i) carefully align the WG
ii) select the portion of the sample to measure and select the incidence angle of the waveguided beam on the sample
iii) measure the diffracted intensity

3.1 Description of the apparatus

The WG diffractometer we will describe is sitting at the beam-line ID13 of the European Synchrotron Radiation Facility (ESRF) in Grenoble (France) and is the result of collaboration between the group at IESS, researchers of synchrotron Elettra (Trieste - Italy) and staff of ID13.
A scheme of the whole set-up is shown in Fig. 6.

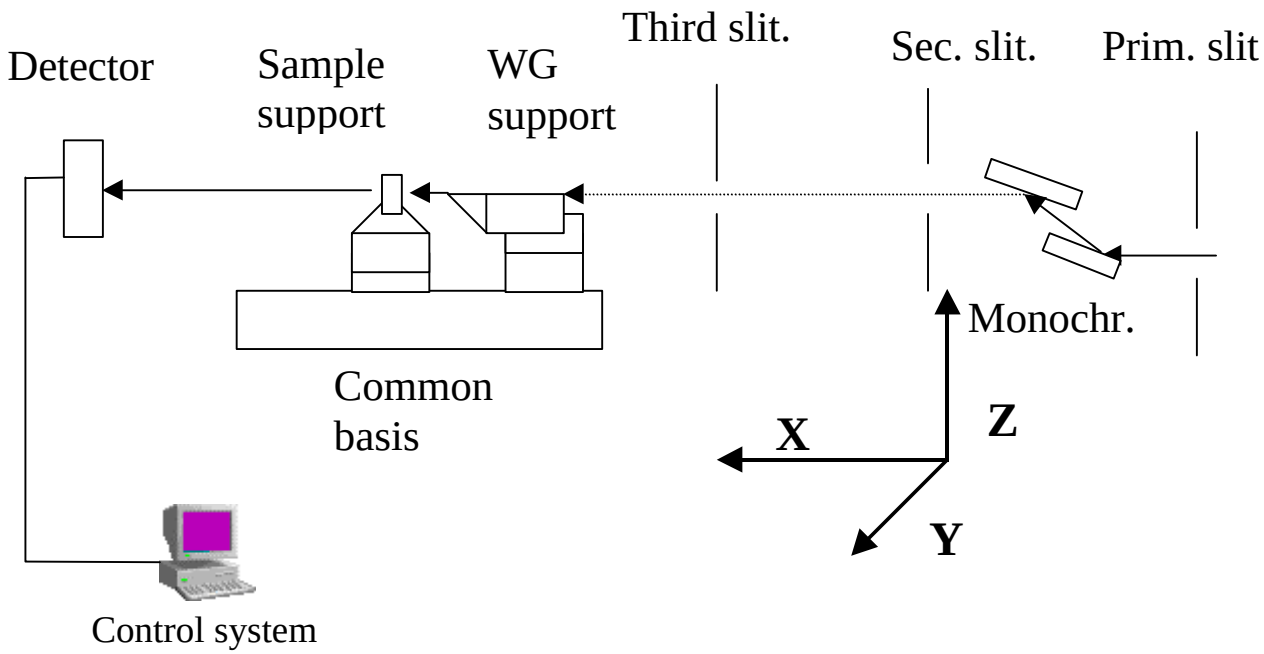

Figure 6; *schematic view of the set-up for micro-diffraction. We can distinguish four basic components: i) beam-line optics and slit system; ii) WG diffractometer; iii) detector system; iv) control system.*

i) **Beam-line optics:** the beam-line optics is composed of a double-crystal monochromator with Si(111) crystals dispersing in the vertical plane. The first crystal is cooled with liquid nitrogen, and a feed-back system keeps the second crystal aligned with the first one. There

are a primary slit system before the monochromator, a secondary slit system after the monochromator, and a third one just before the WG diffractometer. All these have independent control of the horizontal and vertical beam size and position. The monochromator and the primary and secondary slit systems are located in the optics hutch, the third slit system and the WG diffractometer in the experimentsal hutch. Adequate safety systems are in use to prevent accidental irradiation [7].

ii) **WG diffractometer:** the instrument basically is composed of rotation and translation stages separated for the WG and the sample adjustment. The waveguide support has four degrees of freedom (translations along Y and Z, and rotations around X and Y), the sample six degrees of freedom (translations and rotations around all the X, Y and Z axes. The WG and sample have a common basis with six degrees of freedom (hexapode). We call WGTRY, WGTRZ, STRX, STRY and STRZ the translations for WG and Sample along the co-ordinate axes, and WGROTX, WGROTY, SROTX, SROTY and SROTZ the respective rotations around the same axes. The sample has also three high resolution piezoelectric translations along the three co-ordinate axes.

WGROTY controls the angle of incidence of the incoming beam on the WG, and is therefore very critical because the resonance depends on this angle; the rotation is done with a high precision rotation stage with a minimum step of 0.00025° .WGROTX must guarantee the parallelism between the WG edge and the Y axis in about 0.01°. Presently this movement is not motorised, but a rough pre-alignment takes place. WGTRZ is also quite critical because the outgoing intensity strongly depends on the WG height. This movement is done with a translation stage with a limited range of 10 mm and a min. step of 1 μm.

A translation stage of 125 mm range controls WGTRY. With this movement we can change the position of the WG along Y in order to change the point of impact of the incoming beam on the WG.

Concerning the sample movements: STRX and STRY are two high precision translation stages with a range of 100 mm which control the sample position with respect to the WG, with a resolution of 1 μm. Above them is placed a Z stage, STRZ, which changes the sample height with a resolution of 1 μm. On top of it a precision rotation stage, SROTZ with a minimum step of 0.0004° controls the angle of incidence of the beam from the waveguide on the sample diffracting planes. This angle is very critical because if the sample, as usual, is a perfect crystal, its rocking curve can be as narrow as few seconds of arc. On top of SROTZ is placed a goniometer head with the two rotations SROTX and SROTY with a minimum step of about 0.001°. The piezoelectric translations are controlled by a stage called TRITOR. They have 100 μm range with a resolution of 0.1 μm, controlled by an internal feedback system.

In the alignment section we will describe more in detail the purpose of all these movements.

iii) **Detector system**: there are several detectors that have different purposes; an "x-ray eye", which is a very sensitive and fast imaging device with low spatial resolution, is used for fast alignment. A pin diode with a slit in front of it measures the integrated intensity. A high resolution CCD camera (Sensicam) is used to make accurate measurements of x-ray intensity spatially resolved (spatial resolution of the order of 10 μm.) These detectors have independent movements and some of these can also be used simultaneously, because the pin-diode is partially transparent to x-rays of energy > 13 KeV.

iv) **Control system:** nearly all the movements are motorised and remotely controlled by computer. We used the standard application of ESRF (SPEC) both to control the mechanical movements and to acquire data from detectors. Beyond control of movements, we have also optical CCD cameras that are used to precisely place the sample in front of the WG.

Fig. 7 and 8 are pictures of the apparatus.

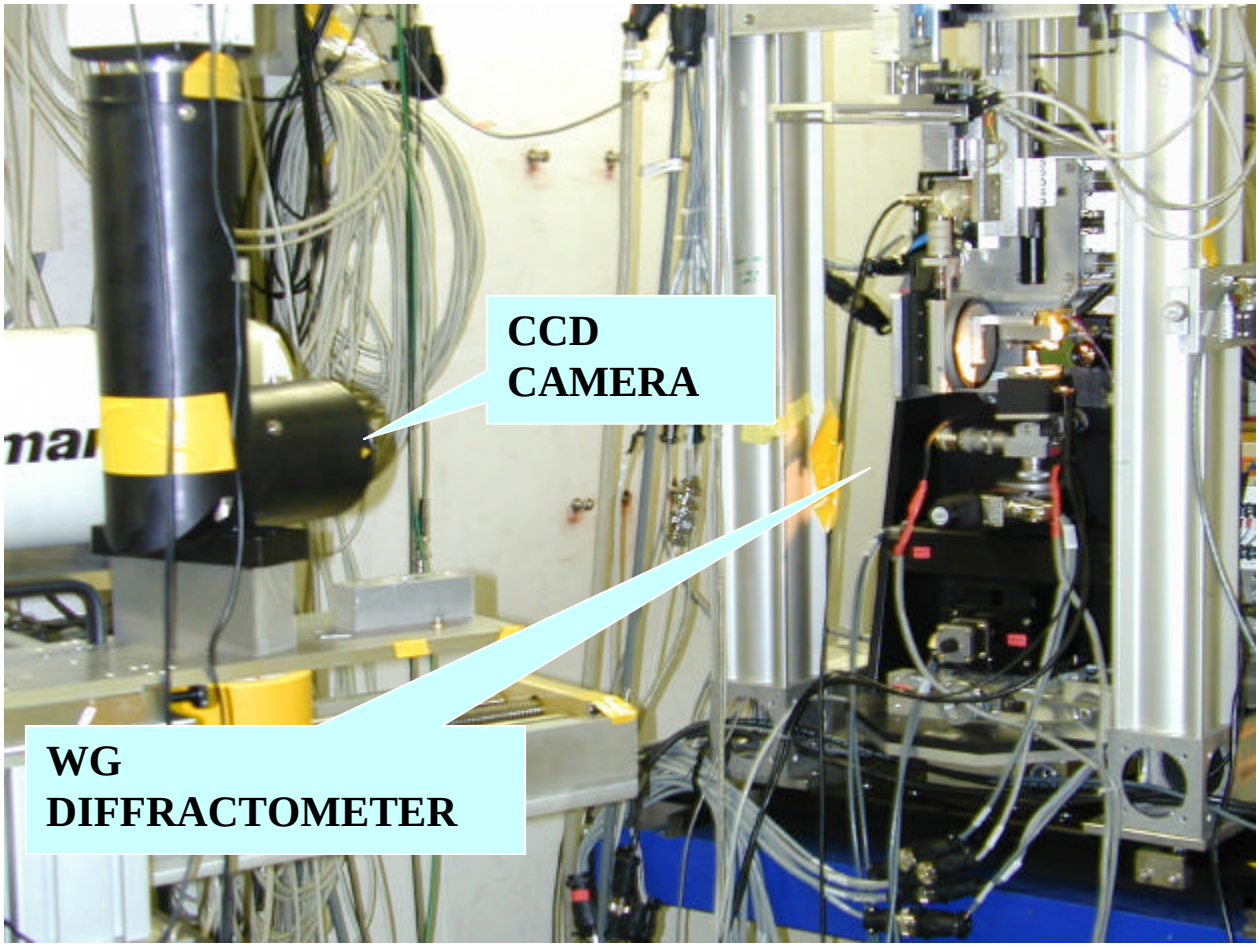

Figure 7. *General view of the apparatus with the detector*

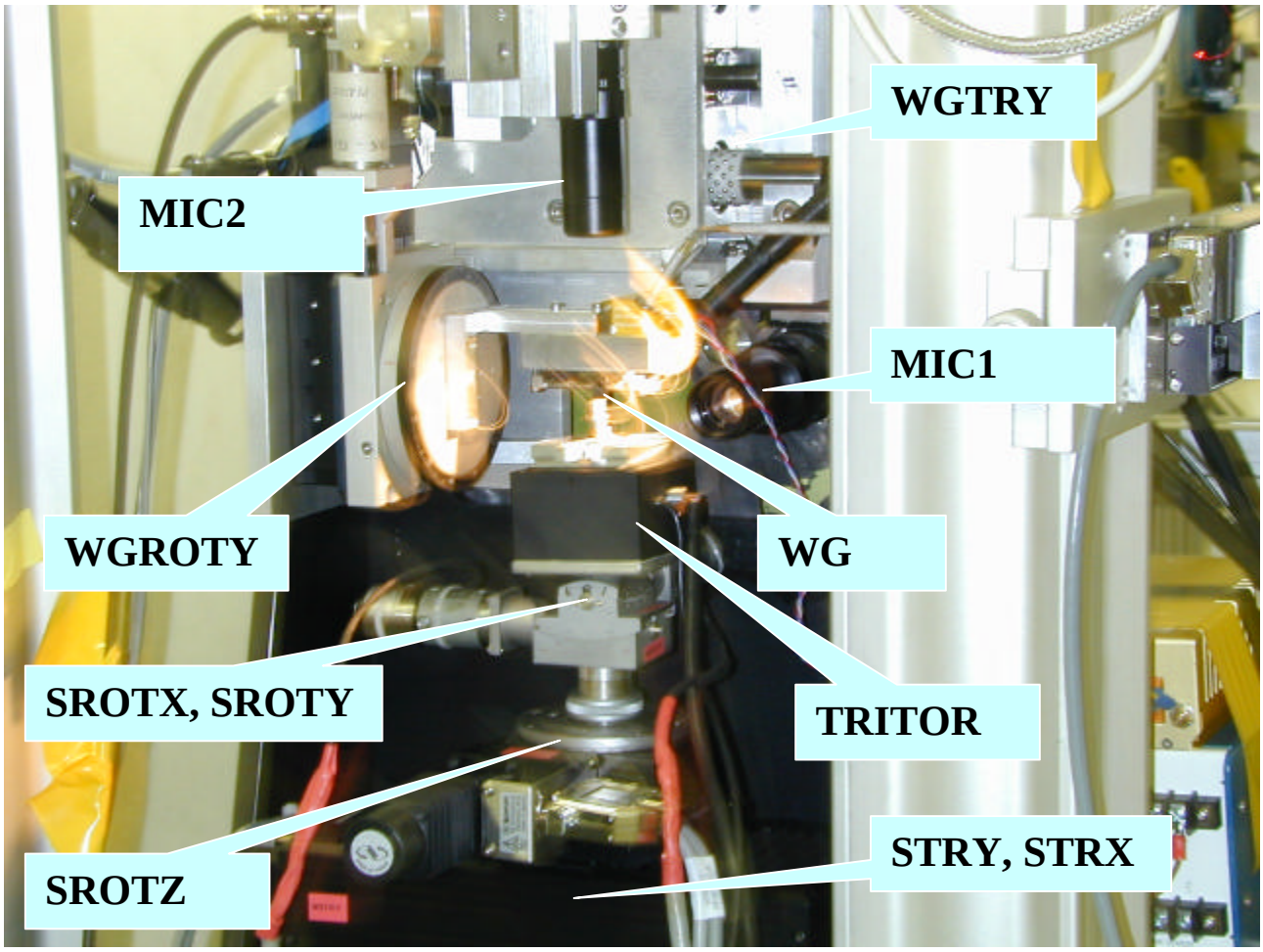

Figure 8. *View of the WG, sample support and alignment microscopes of the WG diffractometer.*

3.2 Alignment procedures

In the alignment procedures we must distinguish between the alignment of the WG and the alignment of the sample. The first task has the purpose to optimise the intensity exiting from the WG, the second one to properly select the portion of the sample illuminated, and the diffracting planes. In many cases it is useful, for a preliminary rough alignment, to have a laser beam which follows the same travel of the x-ray beam.

3.2.1 WG alignment

In order to understand the WG alignment procedures, we must note that after interaction with the WG, we have three beams: the direct (D), the Reflected (R) and the guided (W) ones. Fig. 9 clarifies this important point.

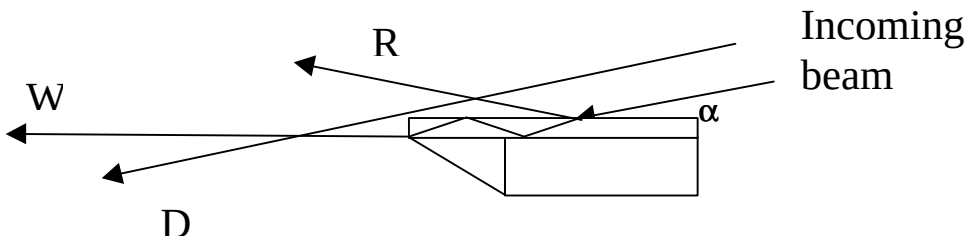

Figure 9. *Sketch of the beams exiting the WG. R = reflected beam; D = Direct beam; W = Waveguided beam*

The direct beam has the same direction of the incoming beam, the reflected makes with it an angle twice the incident angle α, and the guided beam is tangent to the WG surface, thus makes the angle α with the incoming beam. In order to have an intense guided beam, two parameters must be properly adjusted: the angle of incidence α and the WG height. This last parameter is important because determines the distance the beam must travel inside the WG before to exit, and therefore strongly affects the loss for absorption and reflection. In order to facilitate this operation, we determine the angle of resonance through the reflectivity curve that has strong minima in correspondence of it (see Figs 3 and 4). For most of the measurements we want that only the guided beam hits the sample, therefore we placed a cover onto the WG that allows coupling of the incoming beam with the WG structure, but that blocks the direct and reflected beams. Fig. 10 shows schematically the WG with its cover.

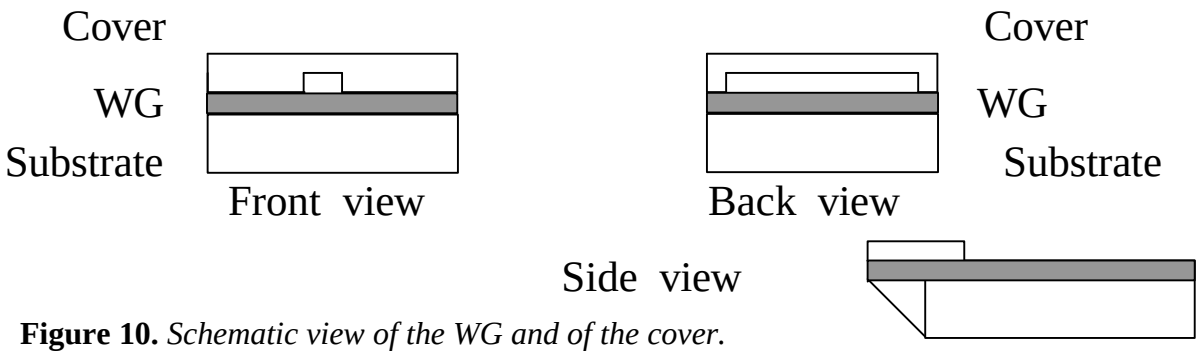

Figure 10. *Schematic view of the WG and of the cover.*

The incoming beam can enter in the space between the WG and the cover, being the grazing angle of the order of few tens of a degree, and couple with the WG. Except in correspondence of a hole in the cover, only the WG beam can exit, the direct and the reflected beams being blocked by the cover. In order to avoid any point of no contact between cover and WG surface, a thin In wire (a very soft material used for sealing) is placed between them. The hole in the front of the cover has an alignment purpose: from it is possible to detect the reflected beam and to determine the angular position (in WGROTY) of the resonance.

The operation is therefore the following:

1) The incoming x-ray beam is optimised as regard to intensity with the monochromator, and its size is determined by means of the third slit system to about 50 μm height and 500 μm wide.
2) We position the WG in order that the incoming beam is in correspondence of the hole in the cover front.
3) With the x-ray eye we determine the height at which the WG surface intercepts the incoming beam.
4) By moving WGROTY we determine the angular position at which a reflected beam is generated (a spot of similar intensity of the incoming beam must appear, which moves vertically when WGROTY is changed).
5) A reflectivity curve is then measured with the pin diode. A slit in front of it blocks the direct beam in order that only the reflectivity is measured.
6) The reflectivity should clearly show minima in correspondence of resonance. WG is then put at the angular position corresponding to first (or in some cases to second) minimum.
7) In order to measure the guided beam we must now close the slit in front of the pin diode and position it to intercept the guided beam. If the pin-diode is at a distance of 100 mm from the WG, then the distance of the guided beam from the reflected beam at the pin-diode position is about 0.2 mm (for a grazing angle of 0.13°). Therefore we close now the pin-diode slit at about 0.15 mm and make a scan in height of the pin-diode. We derive from this the exact position of the direct and reflected beam for that particular angular position of the WG. We place then the pin-diode at the intermediate position between them.
8) In these conditions only the WG height should be adjusted in order to optimise the coupling of the incoming beam with the WG. This is accomplished with WGTRZ. A peak should be measured. Then a check of the best angular position of the WG is carried out. An angular scan can give the output of the different resonance orders. Comparing the intensity of the guided beam with the reflected one give us the measure of the WG efficiency and of the gain.
9) Then we can block the direct and reflected beams moving the WG along Y to a position where the incoming beam is not in correspondence of the hole in the cover. In this case the WG angular and height position must be checked again. Sometimes, however, can be useful to have also the direct and reflected beams. In fact in the projection geometry if the detector is far enough from the WG the images of the three beams are well separated and do not interfere one's another. On the other end the coupling of the incoming beam with the WG is more efficient without the cover and sometimes the presence of the direct and reflected beams can be useful for alignment in diffraction and for calibration purposes.

3.2.2 Sample alignment

Once the WG is aligned we must proceed with the alignment of the sample. The main problem is to select on the sample the particular point we want to measure (for example a given structure) and to precisely place it under the waveguided beam. We must also precisely determine the distance between the sample and the waveguide. We use to this purpose two optical microscopes and an alignment sample. One optical microscope (MIC1) is placed closed to the WG and looks in the

same direction of the incoming x-rays. The other (MIC2) is placed in order to see the WG edge from the top. (see figure 8). The procedure is then the following:

1) An alignment sample such as a knife edge of absorbing material (for ex. Tantalum) is prepared and placed on the sample holder in front of the waveguided beam at a distance $D_1 \approx 5$ mm (roughly measured). With the aid of the microscope MIC2 we visualise the waveguide edge and the sample edge and put this last parallel to the first with SROTZ movement. With relative movements of STRX and measuring the displacement of the image we determine the magnification factor of MIC2 and the distance between the sample and the WG edges.
2) The high resolution CCD camera is placed at a distance $D_2 \approx 500$ mm from the sample in order to detect its radiographic image. The edge is moved in order to intercept the guided beam. Since the detector provides the magnified image of the edge with the magnification
   $M = (D_2 + D_1) / D_1 \approx D_2/D_1 \approx 100$, the corner edge can easily be determined and positioned in the middle of the beam. The horizontal edge can also be placed parallel to the beam. We can then move vertically the sample of a known (small) quantity and measure the displacement in pixel on the CCD camera. Knowing the pixel size it's easy to determine the exact value of the magnification factor. Repeating the measurements for another distance D_1 between sample and waveguide the individual values of D_1 and D_2 can be checked. In this way we obtain absolute values just with relative movements. Also the position on the MIC2 monitor corresponding to the intercept position of the guided beam with the corner edge is determined and noted.
3) The sample is then moved with STRY and STRZ in order to place the corner edge in front of the optical microscope MIC1. Its position on the monitor is then recorded (its image can also be sent to a computer for further image treatment). The distances ΔY and ΔZ the sample must travel to move from the x-ray beam to the optical microscope are noted down. Any other sample we want to measure is then previously placed in front of MIC1 and the structure of interest identified. Then the inverse of ΔY and ΔZ are made in order to put that feature in the middle of the x-ray beam. Repeating this procedure we estimate that the overall precision in positioning is of the order of 2-3 μm. This is large compared with the spatial resolution of the micro-diffraction measurements which is of the order of 100 nm, therefore this alignment procedure must be considered only as a first approximation.
4) The condition for diffraction must then be determined. To this purpose we substitute the knife edge with a perfect Si crystal with the same crystallographic orientation of the sample of interest (in general (001)), and put it in such a way that the x-ray beam makes with its surface roughly the θ_B angle, where θ_B is the Bragg angle for diffraction with that particular photon energy and diffracting planes. Then we look for the diffracted beam either with the pin diode or the x-ray eye, which have a much faster response than the CCD camera. Once found the correct angular position for diffraction with SROTZ, the CCD camera is positioned in order to intercept the beam diffracted at the angle $2*\theta_B$. We must ensure that diffraction takes place in the horizontal plane, and to this purpose we check that the vertical position of the diffracted (waveguided) beam is the same of the direct (waveguided) beam. The angle SROTX is adjusted correspondingly.
5) A diffraction profile (or Rocking Curve, RC) is then recorded with the CCD camera. The sample is rotated through SROTZ within a certain angular range and a given angular step (min. step: 0.0004°). At each angular step the image of the diffracted beam is taken by the CCD camera. An example of the diffracted beam image is shown in fig. 11. We will describe in a later section the procedure to derive the RC from the ensemble of the diffracted images.
6) The sample to measure is substituted to the reference crystal and the structures to analyse (or a reference point) are preliminary visualised with the microscope MIC1. Then the ΔY and ΔZ movements are made in order to bring that feature under illumination of the x-ray beam. We must notice here that the high spatial resolution is only in the Z direction, therefore the most

critical parameter is the determination of the correct height, whilst the Y value is not very critical, because in any case measurements are made on long structures along Y, where we assume a uniform strain. However, it is very important the parallelism between the waveguide and the (long) structures. Therefore it is desirable to have, for example, the structures parallel to the sample edge, in order that further alignment check can be carried out. For example, by means of radiographic procedures similar to those already described, the sample edge can be put parallel to the waveguide edge with high precision (fractions of mrads). Then the procedures for searching of the diffracted beam are carried out, similar to those already described for the perfect sample.

4. Data analysis

4.1 From diffracted images to Rocking Curves

The images are stored in the computer of the control system as a n x m matrix, each element of the matrix bringing the information about the intensity received by a single pixel of the CCD detector. In the experiments we carried out we used two kind of CCD detectors; in one (FRELON camera) the pixel size was 10 μm, in the second (SENSICAM) the pixel size was 6.7 μm. In the following we will refer to the experimental conditions where samples from ST Microelectronics of the 1st campaign measurements were tested. Here the second CCD camera (SENSICAM) was used, at a distance from sample D_2 = 717 mm. For most of the measurements the distance D_1 sample-WG was 5 mm. Considering that the beam from the WG has a gaussian profile with a divergence of about 1 mrad (FWHM) from the WG, the vertical beam size at the CCD camera has a FWHM of about 0.767 mm, corresponding to 114 pixels. In practice enough intensity is also beyond the FWHM, and about 210 pixels can be taken into account. The width of the beam is essentially given by the beam size which in the example considered was 70 μm (FWHM), corresponding to about 10 pixels. Also in the horizontal direction the beam has an intensity profile determined by geometry. The matrix is therefore 210 (rows) x 15 (columns). Fig. 11 shows an example of the diffracted image

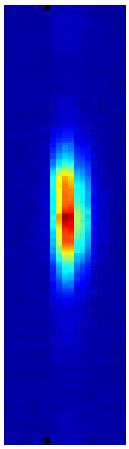

Figure 11. *Example of the diffracted beam image taken by the CCD camera in the case of a perfect Si sample.*

Each row is the contribution from a given spatial region of the sample. With the number given before, D_1 = 5 mm and D_2 = 717 mm, a magnification value M = 145 is obtained (verified by the alignment procedures). This means that a single pixel of 6.7 μm corresponds, in the sample, to a region 46 nm high. The number of columns represent, as said before, the horizontal beam size, but their position in the CCD camera represent the angular position 2θ of the diffracted beam. In fact when we change the angle of incidence of Δω the horizontal position of the diffracted beam changes accordingly of a quantity $2*\Delta\omega*D_2$. The analysis is then carried out row-by-row. Taking the entire set of the diffracted images, and selecting a particular row, we can determine the intensity obtained for each value of ω and 2θ for that particular sample portion. We can therefore analyse these results in terms of reciprocal space, Sx and Sz, through the relations:

$$Sx = 2\sin\theta\sin(\omega-\theta)/\lambda$$
$$Sz = 2\sin\theta\cos(\omega-\theta)/\lambda$$

Where λ is the wavelength of the incoming radiation.
In this way a reciprocal space map can be obtained. This can be repeated for all the rows and therefore spatial variations of structural properties can be put in evidence. Roughly speaking, variations along Sz indicate variations of lattice parameter (Sz = 1/d, where d is the interplanar spacing), whilst variations along Sx indicate bending of diffracting planes. This kind of analysis is therefore very powerful, but derivation of strain from it is not straightforward. On the other side, we noticed that the main variations are in Sz, and that variations in Sx are very limited. We can then integrate in Sx and obtain the intensity as a function of Sz. Fig. 12 is obtained following this quite complex procedure.

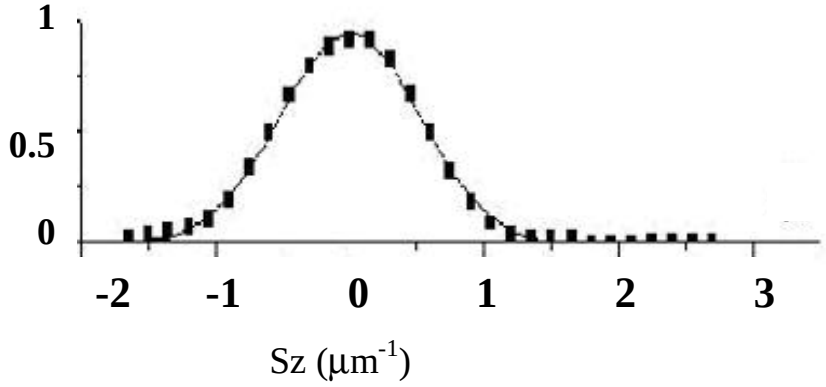

Figure 12. *Rocking curve of the pure Si, as determined from analysis in reciprocal space.*

However, if we assume that the main effect we want to measure is lattice parameter variations, a simpler kind of analysis can be done. In fact, taking an individual diffracted image and integrating on the columns for each row, we obtain the diffracted intensity for a given angular position. Repeating the integration for all the images at the same row value we obtain this intensity as a function of ω, i.e. the rocking curve for that particular row. The result is practically the same than that obtained with the reciprocal space analysis, but the procedure is much simpler and faster. We must notice, however, that the first procedure gives us the assurance that the bending of the diffracting planes is not an important effect. Since this has been verified on the sample we analysed, we will proceed with the simpler data treatment.

The angular width of the RC is determined by convolution among three factors: the intrinsic width that can be calculated by means of dynamical diffraction theory, the horizontal beam divergence and the energy spread of the incoming beam. The intrinsic width, in the standard conditions (Si(400) reflection with 13 KeV) is of the order of 10 μrad. The divergence in the horizontal plane is determined by the slits width and, with a beam size of 100 μm is of the order of 3 μrad. Instead the energy spread, which is of the order of 10^{-4} , gives the largest contribution of about 36 μrad. The RC of the perfect Si crystal, shown in fig. 12, is taken as the instrumental function of our set-up.

4.2 From the measurement to the strain distribution

If the sample is strain-free the same RC must be obtained for all the rows. The only difference is the maximum intensity because, we recall, the guided beam in the vertical direction has a gaussian intensity profile. Is in fact what we obtain for the perfect Si crystal. However, if strain is present in the sample, the RC can be different from row to row. The variations in the RC profile with respect to a reference one give us information on the strain. From Bragg law, an angular displacement $\Delta\theta$ relates to the strain ε (in the direction perpendicular to the planes under consideration) following this simple relation:

$$\Delta\vartheta * \mathrm{cotg}\vartheta_B = -\varepsilon$$

where ϑ_B is the Bragg angle for the set of diffracting planes and the wavelength used.
For planes parallel to the surface, the only ones that we have taken into consideration up to now, the component ε_{zz} is derived. In order to measure the ε_{xx} component, diffraction from planes not parallel to the surface should be considered. This is in principle possible, but for the moment we limit ourselves to the ε_{xx} component. We note here that for uniformity with the standard notations common to the other partners of the consortium, from now on a reference frame connected with the sample is adopted where the co-ordinates X and Y lies in the sample surface, X being transverse to the (long) structures and Y parallel to them, while Z is perpendicular to the sample surface.
It is clear that we must compare the RC from the strained sample (or from the strained region of the sample) with the RC from a perfect Si sample (or from an unstrained region of the same sample). In principle it would be better to compare with a perfect Si sample, but then only the profile could be compared, because the absolute angular position would be lost with the change of sample. It is therefore better to compare the strained part with an unstrained one on the same sample. We can choose a portion far from any structure that can induce strain, but we cannot exclude completely the presence of a strain. We can however compare at least the width of the diffraction profile of the unstrained region with that of a selected strain-free perfect sample. If there is no broadening this means that the strain, if any, is at least uniform in depth. We can also measure the reference profile in different parts of the sample, thus obtaining a sort of averaging, and check that the same profile is obtained for all the rows. Figure 13 shows the rocking curve of a strained part of the sample close to a Shallow Trench Isolation structure in comparison with the unstrained part. It appears clearly that the RC for the strained part is broadened on the low-angle side. This means that an average tensile strain is present for that specific sample portion.
X-rays penetrate deeply into materials, therefore what we obtain is in reality the strain integrated along the sample depth. Therefore from the intensity distribution such that presented in fig. 13 only

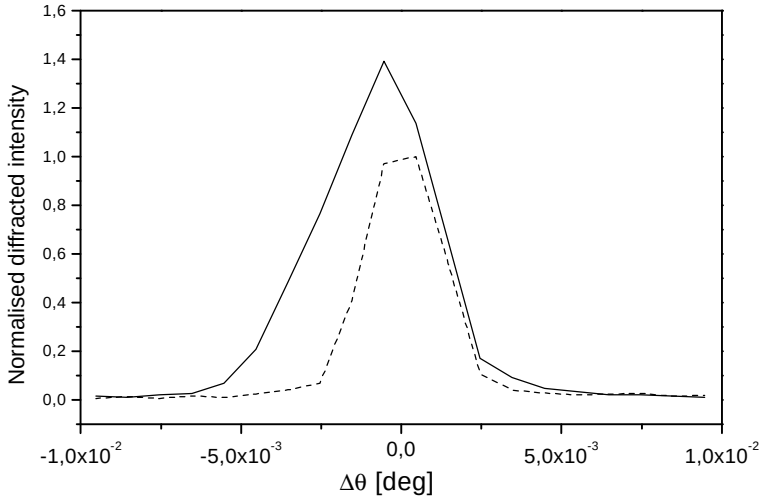

Figure 13. *Rocking curve for a strained (solid line) and an unstrained (dashed line) portions of a sample with Shallow Trench Isolation structures.*

a qualitative information about strain can be derived. In particular we can obtain the sign of the predominant strain and its order of magnitude. With a proper analysis of the intensity distribution, however, we can extract the complete strain depth profile. In order to do this we must have recourse to dynamical diffraction. Very sound and effective theoretical models have been developed which from a given strain depth distribution give the x-ray diffraction profile [8]. We have here the inverse problem, that is we must derive from the diffraction profile the strain depth profile. Since we are not dealing with analytical functions we cannot apply rigorous deconvolution procedures. Therefore we start from a theoretical strain profile, and applying to it the above mentioned dynamical diffraction codes we obtain a diffraction profile that must be compared with the experimental data after a proper convolution with the instrumental function. Then we carry out a fitting procedure which provides us with a refinement of the initial (theoretical) strain depth profile. We performed this kind of analysis on previous measurements with LOCOS structures, in collaboration with C. Giannini of Pastis-Cnrsm, using an analytical model to calculate strain (the Hu model [9]). The result is shown in Fig. 14, where a strain field under a LOCOS structure 1 μm wide is reported. We intend now to proceed in this direction also with the STI structures, using the initial strain profile calculated by the IMPACT code developed by ISEN, a partner of this consortium. This procedure is still under development.

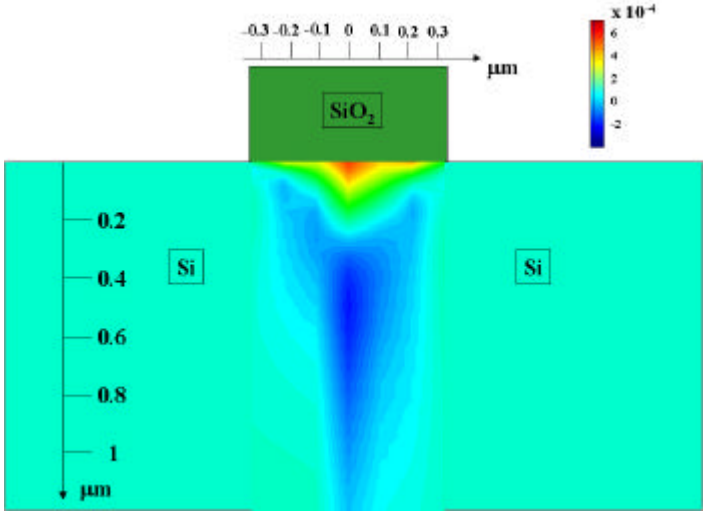

Figure 14. *Strain field under a LOCOS structure determined by comparison of experimental results with theoretical calculation with the Hu model.*

4.3 Considerations on precision, accuracy and spatial resolution.

The x-ray microdiffraction measurements are essentially based on measurements of angular distances from a reference peak, and the factors that influence the precision are essentially the mechanical movements. An estimation of the error they can introduce in the strain measurement is of the order of 10^{-6}

The main factors which affect the accuracy in the strain determination are:

i) the effective x-ray wavelength
ii) the reference diffraction profile
iii) the instrumental function
iv) the fitting procedure

Points i) is not very critical, an estimation gives values of the order of 10^{-6}. Points ii) is more critical. We already discussed this point earlier, and we can estimate that the error introduced by the reference profile is not greater than 10^{-5}.
The instrumental function determines the width of the diffraction profile (both of the strained and unstrained regions). In the present set-up, as already stated, the main contribution to the broadening comes from the wavelength dispersion. The standard band-width of synchrotron radiation beamlines is of the order of 10^{-4}. With the energies and diffracting planes that we generally use this introduces a broadening which is about three times the angular width of the intrinsic diffraction profile. We estimate that this broadening affects the measurement accuracy, mainly for small strain values, giving a limit to the maximum accuracy of the order of $1x10^{-4}$. A significant improvement can be realised with a narrower instrumental function that can be obtained if a non-dispersive geometry for diffraction is set, like the standard double-crystal diffractometer. We plan this improvement for the next run of measurements. The other factor limiting the accuracy is the fitting procedure. We are still working on this subject and is not possible at the moment to give precise values of the accuracy that can be obtained. We can anticipate that the main problem is not the determination of the strain value, that can be quite accurate, but the determination of the depth at which that strain occurs.

The lateral spatial resolution is a function of the waveguide we use and of the magnification. A conservative value of 100 nm has been confirmed by experiments already carried out, but we don't see severe problems to improve this resolution in the future. For example, in the last measurements a magnification of 145 was obtained, leading to a geometric resolution of about 46 nm. However we must also take into account possible errors in alignment that can deteriorate the spatial resolution. For example, if the horizontal beam size is of the order of 100 μm, the projected footprint on the sample is, with the energy and diffracted planes chosen, about 300 μm ($\vartheta_B = 20°$). This means that a disalignment in SROTX of 0.3 mrad deteriorates the spatial resolution of about 100 nm. However, following carefully the procedures described before these misalignment errors can be avoided. Concerning the depth resolution, as explained before, this is related to the fitting procedure that we are working on, and we are not able at the moment to give precise values. We must also give an evaluation of the accuracy in the positioning of the structures. In general the structures we measure are long stripes, symmetric with respect to their median line. If the distance WG-sample is large enough that the entire stripe width is illuminated, one measurement is enough to obtain information on the whole width, and therefore a symmetric feature of the strain with respect to the centre is expected. With the knowledge of the magnification factor through the calibration described before, the distance between specific features gives a quite good accuracy in the determination of the spatial co-ordinates, of the order of few percent of the spatial resolution. In fact, a precise internal

reference frame can be set by letting to coincide the center of symmetry of the strain features with the center of symmetry of the structures.

5. Conclusions

The set-up for micro-diffraction measurements installed at the beam-line ID13 at ESRF has been described in detail, together with the main basis of the technique and of the procedures to properly use the instrument. Some preliminary measurements have been done on samples prepared by ST. These measurements are presented in Del. D8 together with measurements with the other techniques for strain determination (C-BED and micro-raman). Though quite satisfying, improvements in the set-up are possible and desirable, mainly to reduce the broadening due to energy spread. Concerning data analysis, efforts must be made to provide a complete strain depth profile through comparison with theoretical profiles obtained with the IMPACT code. We are working hard in this direction.

6. References

1) S. Lagomarsino et al., J. Appl. Phys., **79**, 4471 (1996)
2) Y.P. Feng, Appl. Phys. Lett., 67, **3647** (1995)
3) J. Wang et al., Science, **258**, 775 (1992)
4) W. Jark et al., J. Appl. Phys., **80**, 4831 (1996)
5) W. Jark et al., Appl. Phys. Lett., **78**, 1192 (2001)
6) S. Di Fonzo et al., Nature, **403**, 638 (2000)
7) http://www.esrf.fr/exp_facilities/ID13/index.html
8) S. Bensoussan et al., J. Appl. Cryst., **20**, 222 (1987)
9) Hu, J. Appl. Phys., **70**, R51 (1991)